Journal of Alloys and Compounds 509 (2011) 7087–7092

Contents lists available at ScienceDirect

Journal of Alloys and Compounds

journal homepage: www.elsevier.com/locate/jallcom

Luminescence properties of Eu^{2+} and Eu^{3+} doped calcium-deficient hydroxyapatite prepared in air

Zhiqiang Feng [a], Yadong Li [a,*], Yanlin Huang [a], Hyo Jin Seo [b,*]

[a] College of Chemistry, Chemical Engineering and Materials Science, Soochow University, Suzhou 215123, China
[b] Department of Physics, Pukyong National University, Busan 608-737, Republic of Korea

ARTICLE INFO

Article history:
Received 21 December 2010
Received in revised form 30 March 2011
Accepted 1 April 2011
Available online 8 April 2011

Keywords:
Calcium-deficient Hydroxyapatite
Precipitation
Luminescence
Eu^{2+}
Eu^{3+}

ABSTRACT

Eu-doped calcium-deficient hydroxyapatite $Ca_{8.95}Eu_{0.05}HPO_4(PO_4)_5OH$ (designated CDHA:Eu) was prepared via the coprecipitation method and calcined in air. Phase purity, crystal structure and morphology of the CDHA:Eu were characterized using X-ray diffraction spectrometer and scanning electron microscopy. The photoluminescence excitation and emission spectra of Eu^{2+} and Eu^{3+} ions were measured using luminescence spectrometer. The emission spectra showed a broad emission band centered at 450 nm corresponded to the typical $4f^65d^1 \rightarrow 4f^7$ transition of Eu^{2+} ions, and sharp peaks corresponded to the $^5D_0 \rightarrow {}^7F_J$ (J = 0, 1, 2, 3, 4) transitions of Eu^{3+} ions. This research was focused on the site-distribution of Eu^{3+} ions. The Eu^{3+} in different sites had different spectroscopic features and the charge compensation mechanisms were also discussed.

1. Introduction

The calcium-deficient hydroxyapatite (designated CDHA), with the Ca/P ratio near 1.5, is structurally and chemically similar to stoichiometric hydroxyapatite (designated HAp, Ca/P = 1.67). The CDHA has greater biological activity than HAp [1] and extensive biological applications such as bone regeneration and bone repair [2–4]. But it is difficult to distinguish between the two closely related calcium apatites using general techniques [5]. The trivalent europium (Eu^{3+}) has been used as a structure probe to investigate the local micro-symmetry of the calcium apatites in previous studies. Silva et al. [6] used the Eu^{3+} ion as a structure probe to characterize the structure of the $Ca_8Eu_2(PO_4)_6O_2$. The Eu^{3+}-doped $Ca_8Eu_2(PO_4)_6O_2$ present a strong and broad excitation band with a maximum at 328 nm, which related to the ligand–metal charge transfer into the hydroxyapatite matrix. The emission spectra of the Eu^{3+}-doped $Ca_8Eu_2(PO_4)_6O_2$ under excitation of 328 nm at room temperature shown the $^5D_0 \rightarrow {}^7F_0$ transition at 573 nm, where it was noticed a slight shoulder at around 572 nm, indicating the presence of two types of spectroscopic sites. Kim et al. [7] investigated the luminescent properties of different solubility Eu^{3+}-doped HAp and β-tricalcium phosphate ($Ca_3(PO_4)_2$, designated β-TCP). It had been shown that the Eu^{3+}-doped HAp exhibited an intense emission at 575 nm and several minor peaks at 610–640 nm. The Eu^{3+}-doped β-TCP had a sharp peak at 613 nm and secondary peaks at 590–600 nm. The more the Eu^{3+} doped, the higher the photoluminescence (PL) intensity was in both cases. Graeve et al. [8] compared the luminescence behavior of Eu-doped CDHA and Eu-doped HAp. For Eu-doped HAp, the emission was obviously from Eu^{3+} ions and corresponded to $^5D_0 \rightarrow {}^7F_J$ (J = 0, 1, 2, 3, 4) transitions, whereas for Eu-doped CDHA, the emission was broad with two peaks at 420 and 445 nm, which corresponds to the $4f^65d^1 \rightarrow 4f^7$ transition of Eu^{2+} ions. The luminescence behavior characterization of the Eu-doped CDHA may be an excellent measure to distinguish between the different calcium apatites. Therefore, the spectroscopic properties of the Eu-doped CDHA and the feasibility of qualitatively determining the Eu-doped CDHA should be further studied.

The objectives of the work were to investigate the charge transfer band, time-resolved emission spectra, site-selective excitation, emission spectra, and decay curves of Eu-doped CDHA, and found out the relationship of the two spectroscopic sties and reduction of the Eu^{3+} ions. The possible charge compensation mechanisms in Eu-doped CDHA were also discussed.

2. Experimental

Eu-doped calcium-deficient hydroxyapatite ($Ca_{8.95}Eu_{0.05}HPO_4(PO_4)_5OH$, designated CDHA:Eu) precursor was prepared via the coprecipitation method. Calcium nitrate tetrahydrate ($Ca(NO_3)_2{\cdot}4H_2O$, Lingfeng, Shanghai) and ammonium hydrogen phosphate ($(NH_4)_2HPO_4$, Lingfeng, Shanghai) were selected for preparing CDHA:Eu precursor. Europium oxide (Eu_2O_3, Yuelong, Shanghai) as a dopant, was dissolved in diluted HNO_3 to obtain $Eu(NO_3)_3$ (0.0285 M) aqueous solution. To prepare $Ca_{8.95}Eu_{0.05}HPO_4(PO_4)_5OH$, the $Ca(NO_3)_2{\cdot}4H_2O$ (0.1 M) aqueous solution was stirred vigorously at 50 °C and then $Eu(NO_3)_3$ and $(NH_4)_2HPO_4$ (0.1 M) aqueous solution

* Corresponding authors.
E-mail addresses: liyadong@suda.edu.cn (Y. Li), hjseo@pknu.ac.kr (H.J. Seo).

0925-8388/$ – see front matter © 2011 Elsevier B.V. All rights reserved.
doi:10.1016/j.jallcom.2011.04.003

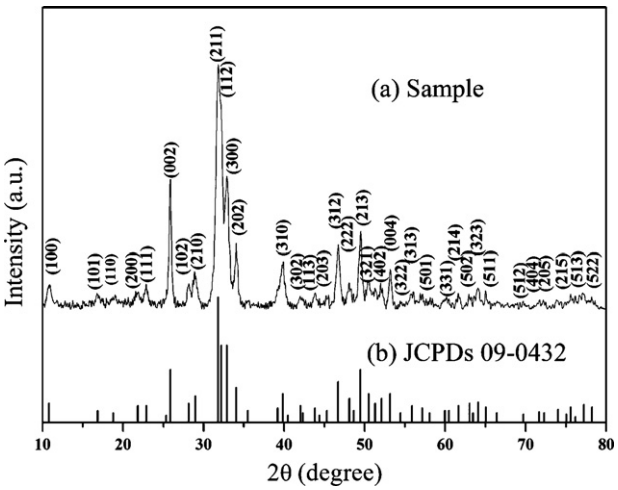

Fig. 1. XRD pattern of CDHA:Eu powders calcined in air and the JCPDs Card No. 09-0432.

were slowly added drop by drop. The pH value of the mixed solution was adjusted to 11 using diluted ammonia solution and the mixture was stirred continuously for 2 h. Coprecipitated powders were filtrated and washed with deionized water to remove residual NO_3^- and NH_4^+ ions and dried at 90 °C. Finally, the powders were heated to 500 °C in 5 min, and then calcined at 600 °C in air for 2 h in a corundum crucible.

The phase purity and crystal structure of the obtained powders were detected by X-ray diffraction (XRD, MERCURY CCD, Japan) using CuKα (λ = 0.15406 nm) radiation in a step-scan mode (0.03° 2θ per step) in the 2θ range 10–80°. The morphologies of the powders were observed using scanning electron microscopy (SEM, S-4700, Hitachi, Japan). The luminescence studies were performed by time-resolved spectra under both selective and non-selective excitation conditions. The excitation spectra and emission spectra were recorded on a Perkin-Elmer LS-50B luminescence spectrometer (USA) with Monk–Gillieson type monochromators and a 20 kW xenon discharge lamp as excitation source. The samples were placed in a liquid helium flowing cryostat for measurements in variable-temperature region (15–300 K). The decay curves were measured using the third harmonic (266 nm) of a pulsed Nd:YAG laser.

3. Results

3.1. Characteristics of coprecipitated powders

Fig. 1 shows the XRD patterns of the coprecipitated powders and the JCPDs Card No: 09-0432. The peaks correspond to those of the stoichiometric hydroxyapatite (HAp), $Ca_{10}(PO_4)_6(OH)_2$. By comparing XRD patterns with JCPDs Card, the formation of Eu-doped calcium-deficient hydroxyapatite during the coprecipitation and calcination reaction in air was confirmed. These Eu-doped calcium-deficient hydroxyapatite powders, designated as CDHA:Eu, possessed a hexagonal symmetry. The calculated lattice parameters of CDHA:Eu were a = 9.425 Å and c = 6.880 Å, which agree with those of CDHA reported by Siddharthan et al. [9]. The coprecipitated CDHA:Eu powders were consisted of crystalline spherical nanoparticles in a size range of 50–150 nm as shown in Fig. 2.

3.2. Luminescence of Eu^{2+} and Eu^{3+}

The emission spectra of the CDHA:Eu under the excitation of 266 nm were measured at 15, 100, and 300 K and shown in Fig. 3. The emission spectra showed a broad band ranging from 400 nm to 500 nm corresponded to the $4f^65d^1 \rightarrow 4f^7$ transition of Eu^{2+} ions and the sharp peaks corresponded to the typical $^5D_0 \rightarrow {}^7F_J$ transitions of Eu^{3+} ions [10].

By enlarging the region of $^5D_0 \rightarrow {}^7F_0$ domain (shown in inset of Fig. 3), the emission spectrum showed two peaks at 574.8 nm and 578.6 nm, respectively. The $^7F_0$ and $^5D_0$ levels were

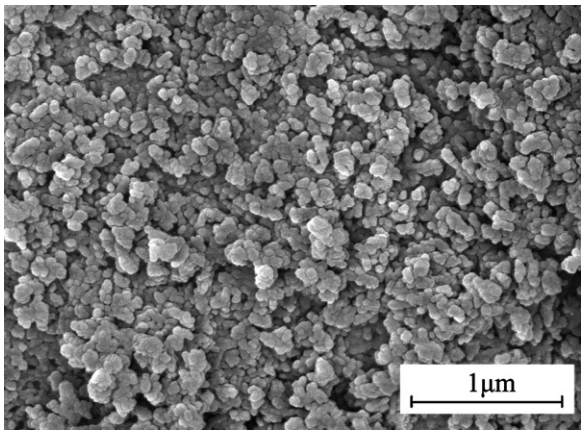

Fig. 2. SEM image of CDHA:Eu powders calcined in air.

non-degenerated. The spectrum associated with the transitions between them should have same number of peaks as the number of non-equivalent sites. Each peak appeared in the spectrum corresponded to a specific Eu^{3+} center since the transition between the non-degenerate $^7F_0$ and $^5D_0$ levels can have only one peak per site [11]. While the occurrence of two emission peaks in CDHA:Eu was consistent with the existence of two types of spectroscopic sites in the host crystal lattice. The two occupations could be confirmed by site-selective luminescence spectra of Eu^{3+}.

The decay curves for the two Eu^{3+} sites in CDHA:Eu were recorded at different temperatures and shown in Fig. 4. The decay curves of $^5D_0 \rightarrow {}^7F_0$ from site Eu_1 exhibited exponential decay which could be fitted into single exponential function:

$$I = I_0 \exp(\frac{-t}{\tau}) \quad (1)$$

where $I(t)$ is the luminescence intensity at time t after the cutoff of the excitation light, I_0 is the initial emission intensity for t = 0, τ is the luminescence lifetime. The decay curves of $^5D_0 \rightarrow {}^7F_0$ from site Eu_2 at different temperatures displayed non-exponential decay, and could be fitted to the effective lifetime defined as the following [12]:

$$\tau_{avg} = \frac{\int_0^\infty tI(t)dt}{\int_0^\infty I(t)dt} \quad (2)$$

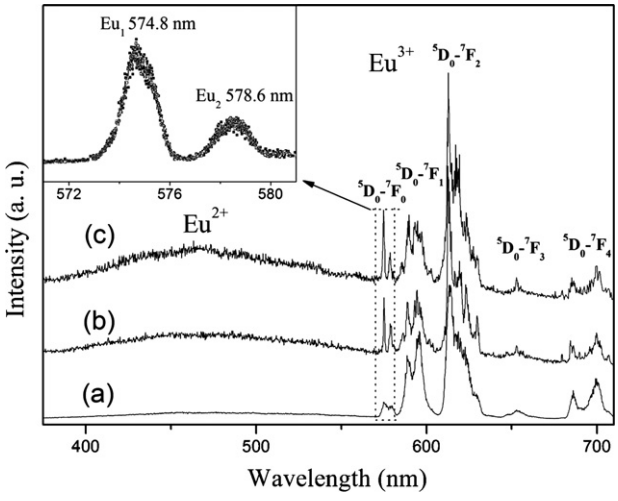

Fig. 3. Emission spectra of the CDHA:Eu under excitation of 266 nm at 15 K (a), 100 K (b), and 300 K (c), respectively. The inset is the enlargement of the emission spectrum corresponding to the $^5D_0 \rightarrow {}^7F_0$ transition at 300 K.

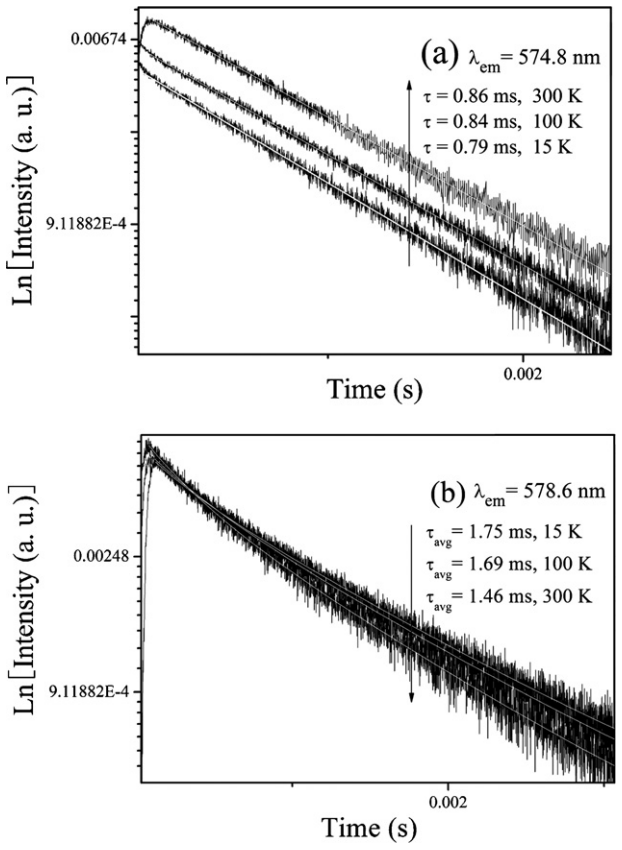

Fig. 4. Decay curves of the $^5D_0 \rightarrow {}^7F_0$ emission at 574.8 nm (a) and 578.9 nm (b) under excitation of 266 nm at different temperatures, 15 K, 100 K, and 300 K, respectively.

The calculated values were showed in Fig. 4. At the same temperature, the lifetimes for Eu^{3+} in site Eu_1 and Eu_2 were 0.79 and 1.75 ms (15 K), 0.84 and 1.69 ms (200 K), and 0.86 and 1.46 ms (300 K), respectively. As the temperature increasing, the lifetime of Eu_2 emission (578.6 nm) decreased, while the lifetime of Eu_1 emission (574.8 nm) increased. The great discrimination of these lifetimes indicated the existence of different luminescence centers of Eu^{3+} ions, and the different spectroscopic sites in CDHA:Eu.

Fig. 5 shows the emission spectrum of CDHA:Eu excited by 266 nm UV light at 300 K with an integrated gate width of 1.33 μs.

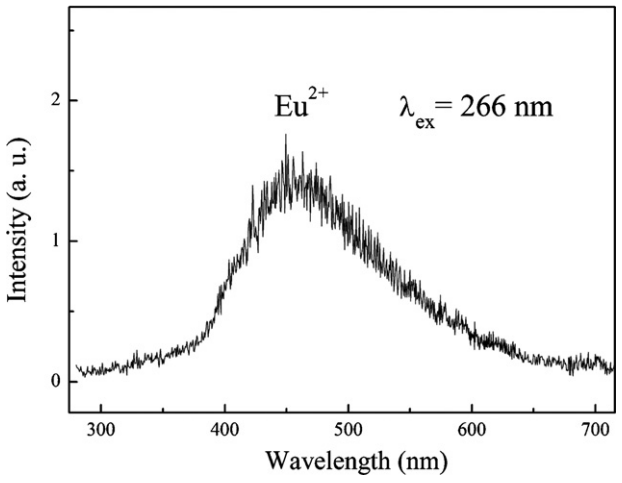

Fig. 5. Emission spectrum of CDHA:Eu under excitation of 266 nm at 300 K with integrated gate width of 1.33 μs.

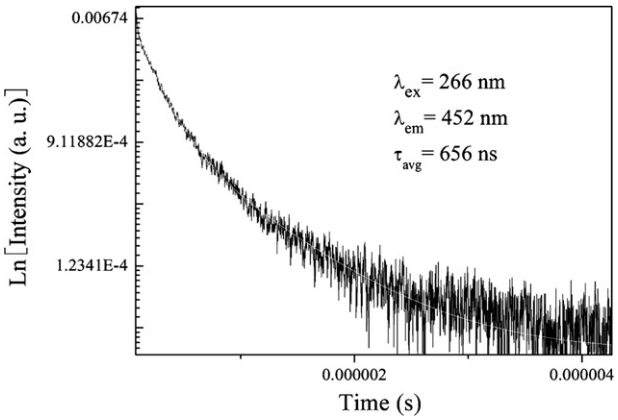

Fig. 6. Decay curve of the Eu^{2+} emission under excitation of 266 nm at 300 K.

The broad emission band located at 450 nm with a shoulder at 400 nm corresponded to the $4f^65d^1 \rightarrow 4f^7$ electric dipole transition of the Eu^{2+} ions in the lattice. As shown in Fig. 6, the decay curve exhibited non-exponential decay with an average lifetime of 656 ns, which was close to the characteristic lifetime of Eu^{2+} ions (τ = 600 ns) in natural apatite [13].

3.3. Charge transfer band of Eu^{3+} ions

The excitation spectra of $^5D_0 \rightarrow {}^7F_0$ emission (Eu_1 and Eu_2) of Eu^{3+} ions in CDHA:Eu were shown in Fig. 7. The dotted lines denoted the Gaussian fitting for the excitation bands (Fig. 7a) with maxima at 260 nm and 320 nm. Only one intense band, at 251 nm, was observed in Eu_2 excitation spectrum (Fig. 7b). Typical charge transfer (charge transfer band, CT band) of the Eu^{3+}–O^{2-} bond in apatites was found in excitation spectra between 220 nm and 360 nm [9]. While, the sharp peaks in the range of 360–420 nm could correspond to the transitions between the ground level $^7F_0$ and the excited levels of $^5D_4$, ^5G_J, $^5L_6$, $^5D_3$ [14].

Under the excitation of CT band at 355 nm, the red emission peak at 574.8 nm, corresponding to the $^5D_0 \rightarrow {}^7F_0$ transition, was the dominant luminescence (Fig. 8a). This spectrum indicated a high value of 12.2 (I_{00}/I_{01}, the ratio of the integrated intensity of $^5D_0 \rightarrow {}^7F_0$ transition to $^5D_0 \rightarrow {}^7F_1$ transition). By comparing the excitation band (Fig. 7), it could be found that the emission peaks under excitation of 355 nm at 300 K were from site Eu_1.

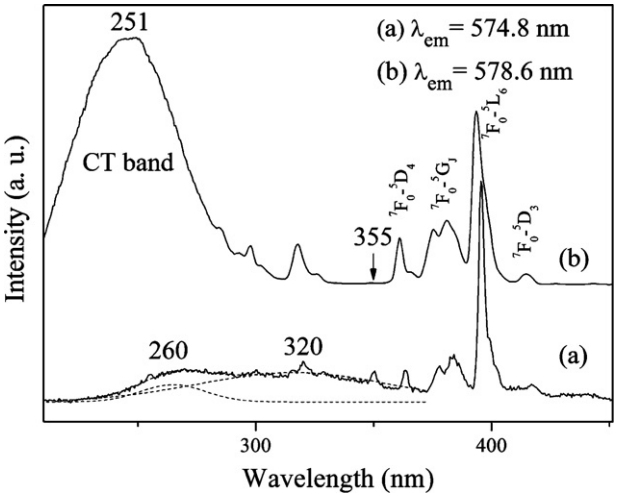

Fig. 7. Excitation spectra of CDHA:Eu by monitoring the $^5D_0 \rightarrow {}^7F_0$ transition at 574.8 nm (a) and 578.6 nm (b) of Eu^{3+} at room temperature.

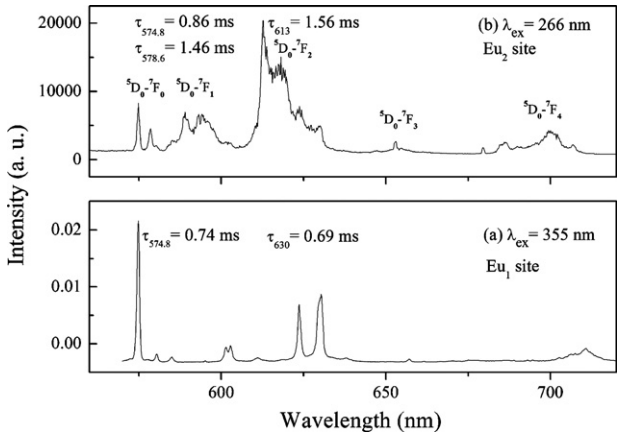

Fig. 8. Emission spectrum of $^5D_0 \rightarrow {}^7F_J$ under excitation of 355 nm (a) and 266 nm (b) in CDHA:Eu at 300 K.

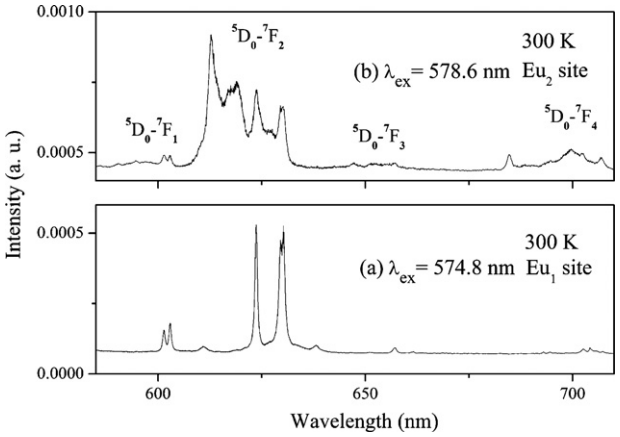

Fig. 10. Site-selective emission spectra of $^5D_0 \rightarrow {}^7F_{1,2,3,4}$ from site Eu_1 exciting at 574.8 nm (a), and that from site Eu_2 exciting at 578.6 nm (b) in CDHA:Eu at 300 K.

As shown in Fig. 8, the lifetimes of $^5D_0 \rightarrow {}^7F_0$ transition under the excitation of 266 nm were 0.86 ms (Eu_1) and 1.46 ms (Eu_2), the lifetime of $^5D_0 \rightarrow {}^7F_2$ transition was 1.56 ms. Under the 355 nm excitation, the lifetime of $^5D_0 \rightarrow {}^7F_0$ was 0.74 ms (Eu_1) and $^5D_0 \rightarrow {}^7F_2$ was 0.69 ms.

3.4. Site-selective emission of $^5D_0 \rightarrow {}^7F_{1,2,3,4}$ transitions

In order to investigate the two sites of Eu^{3+} in CDHA:Eu, the time-resolved emission spectra were recorded at 15 K (Fig. 9). The emission spectra of Eu_1 and Eu_2 had different integrated intensity ratios when recorded with different integrated gate widths. As shown in Fig. 9b, the intensity ratio for site Eu_2 was much higher than the ratio for site Eu_1, which means the lifetime for site Eu_1 was much shorter than the lifetime for site Eu_2.

The site-selective emission spectra of CDHA:Eu were recorded under the excitation of Eu_1 and Eu_2 peaks. The results clearly showed two typical spectra that represent the $^5D_0 \rightarrow {}^7F_{1,2,3,4}$ transitions (Fig. 10). Considering the $2J+1$ components for Eu^{3+} in the crystal field, the maximum splitting of the transition peaks for $^5D_0 \rightarrow {}^7F_{0,1,2}$ were 1, 3, and 5, respectively, for each site. In fact, under the selective excitation at the $^5D_0$ level of Eu_2, the emission spectrum (Fig. 10b) presented six emission peaks for the $^5D_0 \rightarrow {}^7F_1$ transition and more than eight for $^5D_0 \rightarrow {}^7F_2$. Some of the Eu_2 emission peaks were located at the same position of Eu_1 emission peaks.

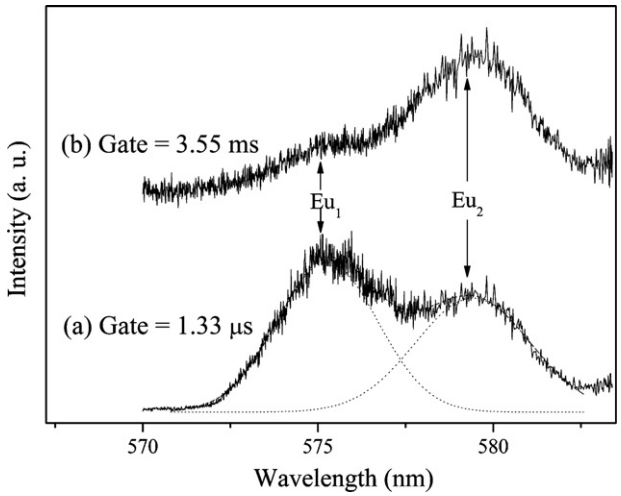

Fig. 9. Emission spectra of CDHA:Eu under excitation of 266 nm at 15 K: (a) integrated gate width of 1.33 μs and (b) integrated gate width of 3.55×10^{-3} s.

Therefore, under the excitation of Eu_2, the $^5D_0 \rightarrow {}^7F_0$ transition emitted peaks from both Eu_1 and Eu_2 sites (Fig. 10b). In this case, by comparing the two spectra in Fig. 10, the Stark components of the $^5D_0 \rightarrow {}^7F_{0,1,2}$ transitions for the two sites of Eu^{3+} in CDHA:Eu could be identified and were listed in Table 1.

The decay curves of $^5D_0 \rightarrow {}^7F_2$ emission were recorded at 300 K from Eu_1 (574.8 nm) and Eu_2 (578.6 nm) and shown in Fig. 11. The decay curve of $^5D_0 \rightarrow {}^7F_2$ emission from Eu_1 showed an exponential decay with a time constant of 0.86 ms at 300 K. However, decay curve from Eu_2 displayed a non-exponential decay with an average time of 1.71 ms. The non-exponential decay might be related to the energy transfer of Eu^{3+} from site to site.

4. Discussion

Calcium apatite has a well-known crystal structure belonging to the *P*63/*m* space group. This structure reveals the existence of two non-equivalent cation sites labeled Ca-I and Ca-II corresponding to the 4f and 6 h positions, respectively. The Ca-I site with C_3 symmetry is surrounded by nine oxygen ions that belong to phosphate groups, and the Ca-II site is sevenfold coordinated (six oxygen ions and one hydroxide ion) with C_s symmetry. The cation in site Ca-II is coordinated to an oxygen ion which presents in the channel (along the *z*-axis) of the apatite [15]. The oxygen ion does not belong to phosphate groups and is sometimes called interstitial oxygen ion ($O^{2-}{}_i$). The open channel can provide enough space to accommodate the interstitial $O^{2-}{}_i$.

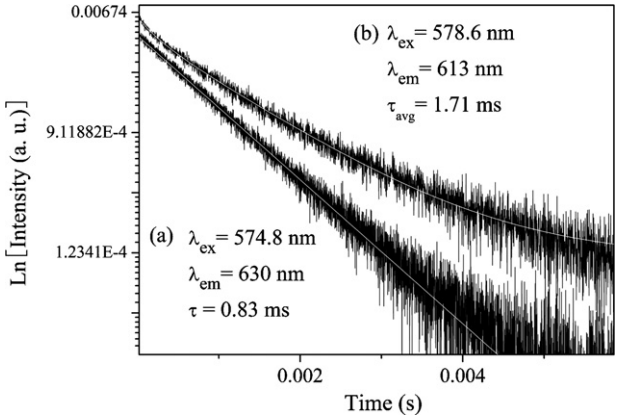

Fig. 11. Decay curves and lifetimes of $^5D_0 \rightarrow {}^7F_2$ emission under excitation in sites Eu_1 (a) and Eu_2 (b) at 300 K.

Table 1
Wavelength (nm) of $^5D_0 \rightarrow {}^7F_{0,1,2}$ transitions for CDHA:Eu and $Ca_5(PO_4)_3F$:Eu [17].

Transition	CDHA:Eu, wavelength (nm)		$Ca_5(PO_4)_3F$:Eu [17], wavelength (nm)	
	Eu^{3+}–Ca^{2+}II site	Eu^{3+}–Ca^{2+}I site	Eu^{3+}–Ca^{2+}II site	Eu^{3+}-Ca^{2+}I site
$^5D_0 \rightarrow {}^7F_0$	574.8	578.6	572	579
	–		577	
$^5D_0 \rightarrow {}^7F_1$	–	589.0	582	588
	601.4	590.3	584	594
	602.9	594.7	597	–
	610.9		613	
$^5D_0 \rightarrow {}^7F_2$	620.9	612.8	622	613
	623.7	617.5	625	618
	629.5	619.0	628	–
	630.2	623.6	630	623
	632.8		632	

The emission spectra (Fig. 3) show that the Eu^{3+} ions are partly reduced to Eu^{2+} in CDHA:Eu. The transitions between the first excited $4f^65d$ state and $4f^7$ ground state ($8S_{7/2}$) are possible and should give very intense emission. While, the emission spectra of f–d transition of Eu^{2+} are usually broad because of large special extension of the 5d wave function and the lattice vibration of the surroundings [10]. Therefore, the broad emission as shown in Fig. 5 corresponds to the typical transition attributed to Eu^{2+} in the CDHA:Eu.

As the temperature increases, the variation in the intensity of emission spectra of Eu^{2+} is consistent with of emission spectra of $^5D_0 \rightarrow {}^7F_0$ from site Eu_1. In this case, it is believed that the Eu^{2+} predominantly occupy the Eu_1 sites. This shows that vacancies could appear in both Ca^{2+} sites and OH^- sites in CDHA crystal structure. The vacancies may cause the distortion of the host crystal lattice structure [3]. CDHA:Eu has a structure that is lack of symmetry due to the calcium deficiency. Thus, further removal of ions from the structure can cause a thermodynamic imbalance and force Eu^{3+} into Eu^{2+} state to keep thermodynamic balance. In other words, the energy required to generate further disorder in the CDHA:Eu structure, so as to accommodate Eu^{3+}, might be too high to promote the necessary charge compensation. The thermodynamic balance will force some Eu^{2+} into Ca^{2+} sites. This phenomenon cannot be found in HAp because the HAp has a symmetry structure which can afford to lose some of Ca^{2+} in order to accommodate the Eu^{3+} ions [8].

The presence of two main sites of Eu^{3+} observed in the spectra (Fig. 3) can be explained by different arrangements of charge-compensating ions and vacancies related to emitting of Eu^{3+} ions. This is consistent with the results of site-selective emission spectra in Fig. 10. When rare earth ions substitute Ca^{2+} ions in calcium apatite, it is believed that Eu^{3+} ions predominantly occupied Ca-II site [16,17]. For example, in the Eu^{3+}-doped calcium hydroxyapatite [18], three distinct spectroscopic sites can be found for $^5D_0 \rightarrow {}^7F_0$ transition. The first two sites are associated with the Eu^{3+} in Ca-II sites and the other one is associated with Eu^{3+} in Ca-I site.

The exceptionally strong intensity of the $^5D_0 \rightarrow {}^7F_0$ transition emission peak (Fig. 8a) has been reported in many literatures. In Eu^{3+}-doped oxyapatites [19], $I_{00}/I_{01} \approx 10$, Eu^{3+} ions predominantly occupy Ca-II site (C_s symmetry). In Eu^{3+}-doped $Ca_{10}(PO_4)_6(OH)_2$:$BO_3{}^{3-}$ [20] apatite, $I_{00}/I_{01} \approx 10$, Eu^{3+} ions also predominantly occupy Ca-II site (C_s symmetry). The interstitial oxygen ions substitute for OH^- ions in the lattice. In this case, the $I_{00}/I_{01} \approx 12.2$ in the CDHA:Eu is similar to their luminescence data. The most possible explanation for this is that Eu^{3+} ions are surrounded by seven oxygen ions from phosphate groups and occupy the Ca-II site. Furthermore, the substitution of Eu^{3+} for the Ca^{2+} ions is necessarily accompanied by a charge compensation mechanism:

$$Ca^{2+} + OH^- \rightarrow Eu^{3+} + O^{2-}{}_i \quad (3)$$

To maintain charge neutrality, interstitial $O^{2-}{}_i$ remains in the positions near Eu^{3+} and replaces the OH^- which locates at the (6 h) channel position. The similar features observed in the emission spectra of Eu^{3+}-doped oxyapatite can be explained by the formation of a covalent bond between Eu^{3+} ion and an interstitial $O^{2-}{}_i$ [19]. Under the site-selective excitation of Eu_1 at 300 K, the emission exhibits an exponential decay with a relative shorter lifetime of 0.83 ms (Fig. 11). This can explain why the Eu^{3+} was strongly perturbed by the oxygen ion from the charge compensation. The relaxation processes for the Eu^{3+} that occupied Eu_1 site are faster. The most possible reason is the formation of the Eu–O bond with interstitial $O^{2-}{}_i$.

Usually, the electric dipolar $^5D_0 \rightarrow {}^7F_2$ transition is very sensitive and the magnetic dipolar $^5D_0 \rightarrow {}^7F_1$ transition is not sensitive to the relative structure changes in surrounding of Eu^{3+} ions. Large splitting of $^5D_0 \rightarrow {}^7F_2$ transition is attributed to the decrease of crystal symmetry. Tanaka et al. [21] reported that in lower symmetry crystal field, the large relative intensity of the $^5D_0 \rightarrow {}^7F_0$ transition should be shifted towards higher energy direction due to the *J*-mixing and the $^5D_0$ level.

On the other hand, the numbers of emission peaks in $^5D_0 \rightarrow {}^7F_2$ transition from site Eu_2 (4 peaks) are less than that from site Eu_1 (5 peaks). The emission spectra under Eu_1 excitation show more pronounced vibronic sidebands, notably in the case of the electric dipole transition of $^5D_0 \rightarrow {}^7F_2$. This indicates that the symmetry of the crystal field in site Eu_2 was higher than that in site Eu_1.

In the Eu^{3+}-doped apatite, the Ca-I site should be weakly occupied because of the long distance between the Eu^{3+} and O^{2-} [22]. The distance is retained when the Ca^{2+} ion is substituted by Eu^{3+} and the intensity of the charge transfer band (CT band) should be higher [23]. As shown in Fig. 7b, the broad band at 251 nm has a higher intensity. While the intense peak at 574.8 nm (Eu_1 site) is attributed to substitution on Ca-II site (C_s symmetry), and the peak at 578.6 nm (Eu_2 site) is attributed to substitution on Ca-I site (C_3 symmetry).

According to the lattice structure, the substitution on Ca-I site may be accompanied by charge compensation mechanism:

$$3Ca^{2+} \rightarrow 2Eu^{3+} + V_{Ca} \quad (4)$$

The decay curves recorded from Eu^{3+} ions located at site Eu_2 are different markedly from those from site Eu_1 (Fig. 11). The de-excitation process for Eu^{3+} in site Eu_2 (1.71 ms) is slower than that of site Eu_1 (0.83 ms). The short lifetime of the site Eu_2 is most probably associated with no Eu–O bond formation. The longer lifetime of Eu^{3+} in site Eu_2 demonstrates that Eu^{3+} does not occupy the Ca-II site and the charge is compensated by the vacancies.

The decay curve of $^5D_0 \rightarrow {}^7F_2$ emission (Fig. 11) from site Eu_1 (Ca-II) is exponential, the decay curve of $^5D_0 \rightarrow {}^7F_2$ emission from site Eu_2 (Ca-I) is non-exponential. This indicates a possible site-to-

site energy transfer. Non-exponential decay curve usually indicated energy transfer from a donor to an acceptor [24]. For example, in the Eu^{3+}-doped strontium fluoroapatites, the Eu^{3+} predominantly occupied Sr-II site (C_S symmetry) and the intense resonant energy transfer from Eu^{3+}(Sr-I) to Eu^{3+}(Sr-II) made the emission from Sr-I site very weak [25]. This means that the energy transfer occurred from Ca-I site to Ca-II site in the CDHA:Eu.

For the Eu-doped CDHA, the rising time for site Eu_1 (Fig. 4a) at 300 K may derive from the effects of unclear defects on the luminescence of Eu^{3+} ions. Based on the present data, it is still difficult to clarify. Further investigations are needed and in progress.

5. Conclusions

The Eu-doped CDHA powders with an average particle size of about 100 nm were successfully prepared using coprecipitation method and calcined at 600 °C for 2 h in air. The luminescence spectra showed that Eu^{3+} ions partly reduce to Eu^{2+} ions in the CDHA:Eu. The emission spectra showed a broad emission band centered at 450 nm that corresponded to the typical $4f^65d^1 \rightarrow 4f^7$ transition of Eu^{2+} ions, and sharp peaks that corresponded to the $^5D_0 \rightarrow {}^7F_J$ transitions of Eu^{3+} ions. Two non-equivalent Eu^{3+} sites labeled Eu_1 (574.8 nm) and Eu_2 (578.6 nm) were attributed to the substitution on Ca-II and Ca-I site respectively. The Eu^{3+} ions might occupy the Ca-II site in C_s symmetry with the charge compensation: $OH^- + Ca^{2+} \rightarrow Eu^{3+} + O^{2-}{}_i$. The charge compensation of Eu^{3+} in the Ca-I site with C_3 symmetry was most probably according to $3Ca^{2+} \rightarrow 2Eu^{3+} + V_{Ca}$ substitution. The formation of Eu–O bonds with the interstitial $O^{2-}{}_i$ was responsible for the relative shorter lifetime of the Ca-II site, and the decay curves of Eu^{3+} ions illustrated the possible energy transfer between the different Eu^{3+} sites.

Acknowledgments

This work was supported by Program for Postgraduates Research Innovation in University of Jiangsu Province (2010), China and by Mid-career Researcher Program through NRF grant funded by the MEST (no. 2009-0078682).

References

[1] S. Sugiyama, T. Minami, T. Moriga, H. Hayashi, K. Koto, M. Tanaka, J. Moffat, J. Mater. Chem. 6 (1996) 459–464.
[2] M. Zheng, D. Fan, X.-k. Li, J.-b. Zhang, Q.-b. Liu, J. Alloys Compd. 489 (2010) 211–214.
[3] N. Kondo, A. Ogose, K. Tokunaga, T. Ito, K. Arai, N. Kudo, H. Inoue, H. Irie, N. Endo, Biomaterials 26 (2005) 5600–5608.
[4] S. Fuchs, X. Jiang, I. Gotman, C. Makarov, H. Schmidt, E.Y. Gutmanas, C.J. Kirkpatrick, Acta Biomater. 6 (2010) 3169–3177.
[5] S.-C. Liou, S.-Y. Chen, H.-Y. Lee, J.-S. Bow, Biomaterials 25 (2004) 189–196.
[6] C. Silva, F. Filho, A. Sombra, I. Rosa, E. Leite, E. Longo, J. Varela, J. Fluoresc. 18 (2008) 253–259.
[7] E.J. Kim, S.W. Choi, S.H. Hong, J. Am. Ceram. Soc. 90 (2007) 2795–2798.
[8] O.A. Graeve, R. Kanakala, A. Madadi, B.C. Williams, K.C. Glass, Biomaterials 31 (2010) 4259–4267.
[9] A. Siddharthan, S. Seshadri, T. Kumar, J. Mater. Sci. Mater. Med. 15 (2004) 1279–1284.
[10] G. Blasse, B.C. Grabmaier, Luminescent Materials, Springer-Verlag, 1994.
[11] C. Görller-Walrand, K. Binnemans, Handbook on the Physics and Chemistry of Rare Earths, vol. 23, 1996, 121–283.
[12] M. Daldosso, D. Falcomer, A. Speghini, P. Ghigna, M. Bettinelli, Synth. Opt. Mater. 30 (2008) 1162–1167.
[13] M. Gaft, R. Reisfeld, G. Panczer, P. Blank, G. Boulon, Spectrochim. Acta A 54 (1998) 2163–2175.
[14] Y. Pan, Q. Zhang, Z. Jiang, Mater. Sci. Eng. B 133 (2006) 186–190.
[15] G. Blasse, J. Solid State Chem. 14 (1975) 181–184.
[16] L. Boyer, B. Piriou, J. Carpena, J. Lacout, J. Alloys Compd. 311 (2000) 143–152.
[17] R. Sahoo, S. Bhattacharya, R. Debnath, J. Solid State Chem. 175 (2003) 218–225.
[18] R. Ternane, M. Trabelsi-Ayedi, N. Kbir-Ariguib, B. Piriou, J. Lumin. 81 (1999) 165–170.
[19] B. Piriou, D. Fahmi, J. Dexpert-Ghys, A. Taitai, J. Lacout, J. Lumin. 39 (1987) 97–103.
[20] R. Ternane, G. Panczer, M. Cohen-Adad, C. Goutaudier, G. Boulon, N. Kbir-Ariguib, M. Trabelsi-Ayedi, Opt. Mater. 16 (2001) 291–300.
[21] M. Tanaka, G. Nishimura, T. Kushida, Phys. Rev. B 49 (1994) 16917–16925.
[22] S. Bodył, Mineralogia 40 (2009) 85–94.
[23] M. Gaft, R. Reisfeld, G. Panczer, S. Shoval, B. Champagnon, G. Boulon, J. Lumin. 72–74 (1997) 572–574.
[24] T. Fujii, K. Kodaira, O. Kawauchi, N. Tanaka, H. Yamashita, M. Anpo, J. Phys. Chem. B 101 (1997) 10631–10637.
[25] R. Jagannathan, M. Kottaisamy, J. Phys.: Condens. Matter 7 (1995) 8453–8466.